Springer

KSME

Journal of Mechanical Science and Technology 24 (5) (2010) 1177~1184
www.springerlink.com/content/1738-494x
DOI 10.1007/s12206-010-0312-9

Load transportation by dual arm robot using sliding mode control †

Nurkan Yagiz*, Yuksel Hacioglu and Yunus Ziya Arslan

Department of Mechanical Engineering, Faculty of Engineering, Istanbul University, 34320 Avcilar, Istanbul, Turkey

(Manuscript Received November 9, 2009; Revised January 26, 2010; Accepted March 4, 2010)

Abstract

In this study, a sliding mode controlled dual arm robotic system was designed. Such multi-arm, collaborative and synchronous robots typically are employed in hazardous situations such as radioactive materials transport explosives disposal and industrial applications. In the present study, a high performance, robust, non-chattering sliding mode controller (SMC) was developed for the purpose of safe load handling, transportation and trajectory realization. First, dynamic equations of robot/load interaction were derived. Then, the robust SMC was designed for the dual arm robotic system. In order to test the robustness of the proposed SMC, parameter variations and external disturbances were introduced to the system. Furthermore, for comparative purposes, the conventional and widely used, PID controller was also applied to the dual arm robot. Significantly, it was found that the SMC made smaller trajectory tracking errors than the PID controller. An overall analysis of the numerical results confirmed that the dual-arm robotic systems with the proposed SMC can safely and effectively be used in hazardous applications.

Keywords: Load transportation; Dual arm robot; Sliding mode control

1. Introduction

Dual arm cooperative robot systems are used in a wide range of industrial applications. This is so mainly because those robotic systems are able to handle large objects and assemble complex industrial parts with high precision as well as reliably, such as in production of metal sheet profiles and welding with heavy machinery on production lines [1-3]. Not surprisingly then, for hazardous tasks such as transportation of active uranium in nuclear power plants or disposal of explosive ordnances, dual-arm robotic systems are frequently preferred [4]. A dual arm robot is more advantageous than the single arm version due to the lesser joint torque requirement for the same task. However, the main disadvantage of using a two-arm robot arises from the necessity of more complex mechanical analysis and control strategy design [5]. The difficulty in mechanical analysis for dual arms comes mainly from the closed chain system, which is formed during the manipulation of the objects, and which is much more kinematically and dynamically complex than the typical serial manipulator configuration [6]. This enhanced complexity is due also to the additional requirements of maintaining a grasp and the necessity to coordinate dynamic interaction between the robot arms [7].

In order to ensure a good tracking performance on the robot trajectory, it is required that a controller be employed to coordinate the arms synchronously. Uchiyama et al. [8] applied a hybrid control technique to a two-arm industrial robot. Laroussi et al. [9] considered linear state feedback for stabilization and control of two planar robots in lifting a load and transporting it to a new location. Lin and Huang [10] presented a fuzzy force control framework for object handling with a dual industrial robotic system. However, unexpected disturbances and obstacles can occur in the robot system's workspace or task environment. In these circumstances, maintaining the desired motion trajectory requires the use of a robust and reliable controller. Thus, the sliding mode controller (SMC) was investigated in the present study.

The variable structure SMC has enjoyed widespread use and attention since the paper by Utkin [11]. In this control method, the states of the system are directed to reach a predefined sliding surface after which they are maintained on that surface by means of a sliding motion. While sliding, the system is insensitive to parameter variations and external disturbances. In fact, it is on account of the SMC's robust behaviour, that it has found a wide applications in industry, ranging from robotic manipulator control [12, 13] to control of mobile robots [14, 15], process control [16], flight control [17], and so on. However, the classical SMC suffers from chattering, which is due generally to the discontinuous term included in

† This paper was recommended for publication in revised form by Associate Editor Doo Yong Lee

*Corresponding author. Tel.: +90 212 473 70 48, Fax.: +90 212 473 71 80
E-mail address: nurkany@istanbul.edu.tr

the control signal, and which can be harmful to the mechanical components of the system. One way to eliminate this problem is to replace the discontinuous signum function in the control signal with a saturation [18] or sigmoid like function [19]. For example, fuzzy-inference-obtained continuous approximation is one solution that has been employed [20]. In the present study, chattering was avoided by designing the controller without a discontinuous term.

The aim of this study was to investigate the performance of two coordinated planar sliding mode controlled arms in transporting a load to its new location with friction-assisted handling. Since these robotic systems are widely used in hazardous environments, robust SMC was preferred in this study which provides efficient tracking performance. The rest of the paper is organized as follows. In Section 2, the physical model of the dual arm robotic system is presented. In Section 3, the SMC methodology is introduced. in Section 4, the numerical test results are discussed, and finally, in Section 5, conclusions are drawn.

2. Physical model

A model of the cooperative robotic system consisting of two planar robot arms with actuating motors at the revolute joints is illustrated in Fig. 1. The system has four degrees of freedom (DoF). When the system handles an object, the DoF reduces to two, owing to the constraints. Note that the load is not allowed to rotate. In the physical model of the robotic system, m_i, I_i and L_i (i = 1,2,3,4) represents the mass, mass moment of inertia and length of the related links, respectively. Here, k_i is the distance of the center of mass of each link to the preceding joint and θ_i is the joint angle of the related link. Additionally, $m(t)$ is the mass of the load, and d_1 and d_2 denote the width of the rectangular load and the distance between the bases of the robot arms. Also, there is viscous frictions acting on all of the joints denoted by b_i. The numerical values of the parameters were given in the Appendix.

The robot arms move in the horizontal xy-plane and gravity acts in the negative z-direction. There are two periods of robotic motion. First, the robots start from their home position and move towards the rectangular load. Then, the robots handle the load and transport it to its new position while tracking the given trajectory as seen in Fig. 2.

In order to perform the transportation task, the robot arms apply forces F_1, F_2 from the arm tips to the load (Fig. 3). Friction-assisted handling prevents slippage of the load from the contact points during motion. The friction forces F_{s1}, F_{s2} and their components F_{s1y}, F_{s1z}, F_{s2y}, F_{s2z} between the arm tips and the load surface are shown in Fig. 3. Here μ represents the coefficient of dry friction. In this study it was deemed that the load be moved without rotation. Thus, F_{s1y} and F_{s2y} were equal, preventing rotation about the z-axis. F_{s1z} and F_{s2z} also were equal, since there was to be no rotation about the y-axis, either. Then:

$$F_{s1y} = F_{s2y} \tag{1}$$

$$F_{s1z} = F_{s2z} = m(t)\,g/2 \tag{2}$$

The equations of motion after handling the load were given as

$$\begin{aligned}&\ddot{\theta}_1(A_1 + A_2 + 2A_3\cos\theta_2) + \ddot{\theta}_2(A_2 + A_3\cos\theta_2)\\ &-A_3\sin\theta_2(\dot{\theta}_2^{\,2} + 2\dot{\theta}_1\dot{\theta}_2) + b_1\dot{\theta}_1\\ &= u_1 - F_1[L_1\sin\theta_1 + L_2\sin(\theta_1+\theta_2)]\\ &-F_{s1y}[L_1\cos\theta_1 + L_2\cos(\theta_1+\theta_2)] + w_1\end{aligned} \tag{3}$$

$$\begin{aligned}&A_2\ddot{\theta}_2 + \ddot{\theta}_1(A_2 + A_3\cos\theta_2) + A_3\dot{\theta}_1^{\,2}\sin\theta_2 + b_2\dot{\theta}_2\\ &= u_2 - F_1L_2\sin(\theta_1+\theta_2) - F_{s1y}L_2\cos(\theta_1+\theta_2) + w_2\end{aligned} \tag{4}$$

$$\begin{aligned}&\ddot{\theta}_3(A_4 + A_5 + 2A_6\cos\theta_4) + \ddot{\theta}_4(A_5 + A_6\cos\theta_4)\\ &-A_6\sin\theta_4(\dot{\theta}_4^{\,2} + 2\dot{\theta}_3\dot{\theta}_4) + b_3\dot{\theta}_3\\ &= u_3 + F_2[L_3\sin\theta_3 + L_4\sin(\theta_3+\theta_4)]\\ &-F_{s2y}[L_3\cos\theta_3 + L_4\cos(\theta_3+\theta_4)] + w_3\end{aligned} \tag{5}$$

$$\begin{aligned}&A_5\ddot{\theta}_4 + \ddot{\theta}_3(A_5 + A_6\cos\theta_4) + A_6\dot{\theta}_3^{\,2}\sin\theta_4 + b_4\dot{\theta}_4\\ &= u_4 + F_2L_4\sin(\theta_3+\theta_4) - F_{s2y}L_4\cos(\theta_3+\theta_4) + w_4\end{aligned} \tag{6}$$

where A_j (j = 1,2,…,6) are the constant coefficients given in

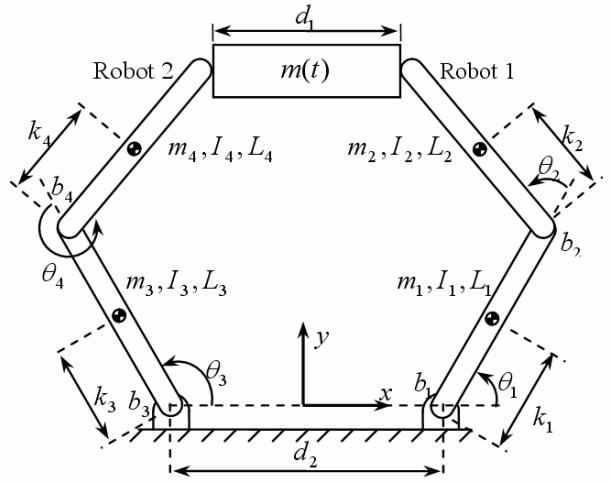

Fig. 1. Physical model of the robot arms.

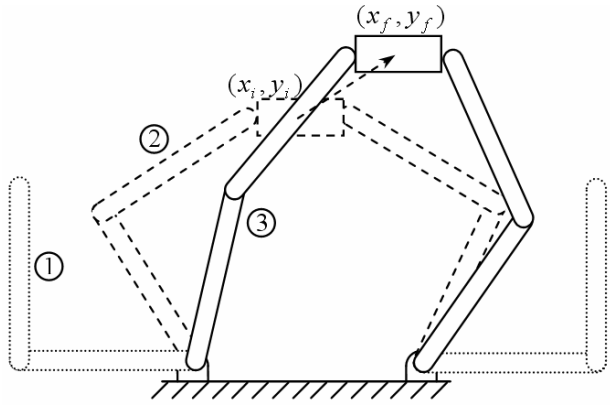

Fig. 2. Motion of the robot arms.

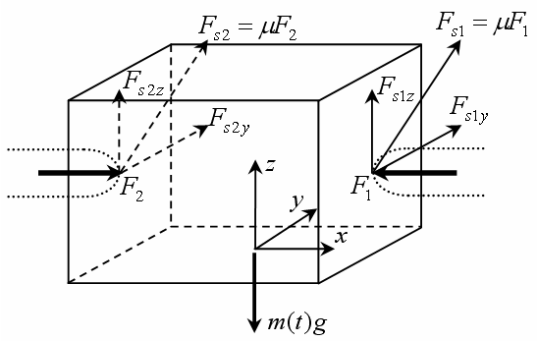

Fig. 3. Representation of forces acting on load.

the Appendix, u_i (i = 1,2,3,4) are the control torque inputs and w_i are external disturbance torques.

Since the x, y coordinates of the center of mass are commonly-employed in defining the trajectory of both arms, the DoF of the overall system reduces to two.

$$\begin{aligned} x_m &= \frac{d_2}{2} + L_1\cos\theta_1 + L_2\cos(\theta_1+\theta_2) - \frac{d_1}{2} \\ &= -\frac{d_2}{2} + L_3\cos\theta_3 + L_4\cos(\theta_3+\theta_4) + \frac{d_1}{2} \end{aligned} \tag{7}$$

$$\begin{aligned} y_m &= L_1\sin\theta_1 + L_2\sin(\theta_1+\theta_2) \\ &= L_3\sin\theta_3 + L_4\sin(\theta_3+\theta_4) \end{aligned} \tag{8}$$

The dynamic equations of the load are:

$$m(t)\ddot{x}_m = F_2 - F_1 \tag{9}$$

$$m(t)\ddot{y}_m = 2F_{s1y} = 2F_{s2y} \tag{10}$$

and the expressions for friction forces are:

$$F_{s1y}{}^2 + \left(\frac{m(t)g}{2}\right)^2 < (\mu F_1)^2 \tag{11}$$

$$F_{s2y}{}^2 + \left(\frac{m(t)g}{2}\right)^2 < (\mu F_2)^2 \tag{12}$$

Since the direction of the forces F_1 and F_2 are always set towards the load so that the load can be effectively handled, these forces should be positive. Therefore, the friction force equation, which yields a positive signed solution for both F_1 and F_2, should be chosen. In this study the following solutions were used. If the acceleration of the load in the x-direction is equal to or greater than zero ($\ddot{x}_{m(t)} \geq 0$), then using Eq. (11), the following relations for F_1 and F_2 are obtained.

$$F_1 = \frac{1}{\mu}\sqrt{\left(\frac{m(t)\ddot{y}_{m(t)}}{2}\right)^2 + \left(\frac{m(t)g}{2}\right)^2} \tag{13}$$

$$F_2 = \frac{1}{\mu}\sqrt{\left(\frac{m(t)\ddot{y}_{m(t)}}{2}\right)^2 + \left(\frac{m(t)g}{2}\right)^2} + m(t)\ddot{x}_{m(t)} \tag{14}$$

Here, since $\ddot{x}_{m(t)} \geq 0$ is satisfied, the interaction forces F_1 and F_2 are both positive. If $\ddot{x}_{m(t)} < 0$, Eq. (12) is used and the following relations for the interaction forces are obtained.

$$F_1 = \frac{1}{\mu}\sqrt{\left(\frac{m(t)\ddot{y}_{m(t)}}{2}\right)^2 + \left(\frac{m(t)g}{2}\right)^2} - m(t)\ddot{x}_{m(t)} \tag{15}$$

$$F_2 = \frac{1}{\mu}\sqrt{\left(\frac{m(t)\ddot{y}_{m(t)}}{2}\right)^2 + \left(\frac{m(t)g}{2}\right)^2} \tag{16}$$

Here, since $\ddot{x}_{m(t)} < 0$ is satisfied, the interaction forces F_1 and F_2 are both positive.

3. Controller design

In sliding-mode-controlled systems, the control input is changed according to predefined rules, which drives, and maintains the system states on a sliding surface. Therefore, for the SMC, there are two steps in the design. The first is to define the sliding surface in the state space, and the second is to obtain the control law in order to construct and maintain the intended sliding motion. In the course of the sliding motion the system is insensitive to parameter variations and external disturbances. A general representation of such sliding motion on the phase plane for a second order system is given in Fig. 4. Besides its invariance properties the classical SMC has a drawback called chattering, which is due mainly to the discontinuous term included in the control law, namely the signum function. This discontinuous control signal in fact can harm the mechanical components of the system. Therefore in the present study, the control law was designed without the signum function, effecting a non-chattering control signal.

The state space form of a non-linear dynamic system can be written as

$$\dot{\boldsymbol{\phi}} = \mathbf{f}(\phi) + [B]\,\mathbf{u} \tag{17}$$

where $\boldsymbol{\phi} = [\phi_1,\ldots,\phi_n,\phi_{n+1},\ldots,\phi_{2n}]^T$. The second half of the states are the time derivatives of the first half for mechanical systems, respectively. $2n$ is the number of states. In Eq. (17), $\mathbf{f}(\phi)$ is the $2n\times1$ vector of the state equations without the control inputs which may include non-linearities, $\mathbf{u}$ is an $n\times1$ generalized torque input vector and $[B]$ is a $2n\times n$ matrix the elements of which are the coefficients of the generalized control inputs in the state equations. For the first arm of the dual arm robot system, by choosing the state variables as $\left[\phi_{1(1)}\,\phi_{2(1)}\,\phi_{3(1)}\,\phi_{4(1)}\right]^T = \left[\theta_1\,\theta_2\,\dot{\theta}_1\,\dot{\theta}_2\right]^T$ and the control input as $u_{(1)} = [u_1\ u_2]^T$ the equations of motion can be arranged in the form of Eq. (17). Similarly, for the second robot arm by defining the state variables as $\left[\phi_{1(2)}\,\phi_{2(2)}\,\phi_{3(2)}\,\phi_{4(2)}\right]^T = \left[\theta_3\,\theta_4\,\dot{\theta}_3\,\dot{\theta}_4\right]^T$ and the control input vector as $u_{(2)} = [u_3\,u_4]^T$ the equations of motion for arm also can be arranged in the form of Eq. (17). Here, the subscripts (1) and (2) in the state variables

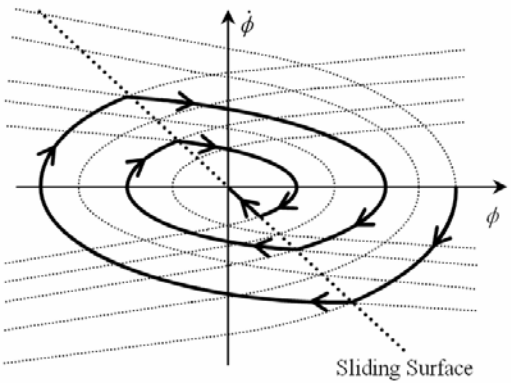

Fig. 4. Representation of sliding motion for a second order system.

stand for the first and second robot, respectively. Therefore, the controller design for the robot arms can be treated separately, and for presentational clarity, the subscripts (1) and (2) are not used here in the discussion of the controller design. The sliding surface was defined as

$$S = \{\boldsymbol{\phi} : \boldsymbol{\sigma}(\phi, t) = 0\}. \tag{18}$$

For a control system, the sliding surface can be selected as

$$\boldsymbol{\sigma} = [G]\,\Delta\boldsymbol{\phi}. \tag{19}$$

Here

$$\Delta\boldsymbol{\phi} = \boldsymbol{\phi}_r - \boldsymbol{\phi} = [\mathbf{e}\ \mathbf{de}/\mathrm{dt}]^{\mathrm{T}} \tag{20}$$

is the difference between the reference value and the system response. [G] includes the sliding surface slopes

$$[G] = \begin{bmatrix} \lambda_1 & 0 & 0 & 0 & 0 & 1 & 0 & 0 & 0 & 0 \\ 0 & \ddots & 0 & 0 & 0 & 0 & \ddots & 0 & 0 & 0 \\ 0 & 0 & \lambda_i & 0 & 0 & 0 & 0 & 1 & 0 & 0 \\ 0 & 0 & 0 & \ddots & 0 & 0 & 0 & 0 & \ddots & 0 \\ 0 & 0 & 0 & 0 & \lambda_n & 0 & 0 & 0 & 0 & 1 \end{bmatrix}_{n\times 2n} \tag{21}$$

for which λ_i is the slope parameter representing the negative value of the each related sliding surface slope,

$$\boldsymbol{\sigma}_i = \lambda_i \mathbf{e_i} + \dot{\mathbf{e}}_\mathbf{i}. \tag{22}$$

For overall stability, the following Lyapunov function candidate has to be positive definite and its derivative has to be negative semi-definite.

$$\mathbf{v}(\boldsymbol{\sigma}) = \frac{\boldsymbol{\sigma}^{\mathbf{T}}\boldsymbol{\sigma}}{2} > 0 \tag{23}$$

$$\frac{\mathrm{d}\,\mathbf{v}(\boldsymbol{\sigma})}{\mathrm{dt}} = \frac{\dot{\boldsymbol{\sigma}}^{\mathbf{T}}\boldsymbol{\sigma}}{2} + \frac{\boldsymbol{\sigma}^{\mathbf{T}}\dot{\boldsymbol{\sigma}}}{2} \le 0 \tag{24}$$

If the limit condition is applied to Eq. (24), the sliding mode condition is obtained as

$$\frac{\mathrm{d}\boldsymbol{\sigma}}{\mathrm{dt}} = \frac{\mathrm{d}\mathbf{A}(t)}{\mathrm{dt}} - [G]\frac{\mathrm{d}\boldsymbol{\phi}}{\mathrm{dt}} = 0 \tag{25}$$

where

$$\mathbf{A}(t) = [G]\boldsymbol{\phi}_r. \tag{26}$$

From Eqs. (17) and (25)

$$\frac{\mathrm{d}\mathbf{A}(t)}{\mathrm{dt}} - [G]\left(\mathbf{f}(\phi) + [B]\,\mathbf{u}_{eq}\right) = 0 \tag{27}$$

where $\mathbf{u}_{eq}$ is the equivalent control torque input vector for the limit condition. Finally equivalent control is found with

$$\mathbf{u}_{eq}(t) = [GB]^{-1}\left(\frac{\mathrm{d}\mathbf{A}(t)}{\mathrm{dt}} - [G]\mathbf{f}(\phi)\right). \tag{28}$$

Equivalent control is valid only on a sliding surface, and so an additional term needs to be defined to pull the system to the surface. Since the design with the classical Lyapunov derivative suffers from chattering, the present study trialled a new candidate derivative that enables chattering-free dual-arm robot control. The new derivative of the Lyapunov function can be selected according to

$$\dot{\mathbf{v}} = -\boldsymbol{\sigma}^{\mathbf{T}}[\Gamma]\boldsymbol{\sigma} < 0. \tag{29}$$

Then, by equating (24) to (29)

$$\boldsymbol{\sigma}^T\dot{\boldsymbol{\sigma}} = -\boldsymbol{\sigma}^T[\Gamma]\boldsymbol{\sigma} \tag{30}$$

$$\frac{d\boldsymbol{\sigma}}{dt} + [\Gamma]\boldsymbol{\sigma} = 0. \tag{31}$$

By taking the derivative of Eq. (19) and using $\dot{\phi}$ from Eq. (17)

$$\frac{\mathrm{d}\mathbf{A}(t)}{\mathrm{dt}} - [G]\left(\mathbf{f}(\phi) + [B]\mathbf{u}\right) + [\Gamma]\boldsymbol{\sigma} = 0 \tag{32}$$

$$\mathbf{u} = [GB]^{-1}\left(\frac{\mathrm{d}\mathbf{A}(t)}{\mathrm{dt}} - [G]\mathbf{f}(\phi)\right) + [GB]^{-1}[\Gamma]\,\boldsymbol{\sigma}. \tag{33}$$

With $\mathbf{u}_{eq}$, the control law given in Eq. (28), the total control input is found by

$$\mathbf{u}(t) = \mathbf{u}_{eq}(t) + [GB]^{-1}[\Gamma]\,\boldsymbol{\sigma} \tag{34}$$

$[GB]^{-1}$ is always invertible and equal to the mass matrix for mechanical systems. [Γ] is a positive definite matrix, and the values of its entries are determined by trial and error at the design stage. However, if $\mathbf{f}(\phi)$ and [B] are not known exactly, the calculated equivalent control inputs will be completely different from the actual equivalent control inputs. Thus, in this study, it was assumed that the equivalent control is the average of the total control [21]. For estimation of the equivalent con-

trol, an averaging filter, here a low pass filter, can be designed as follows

$$\tau \dot{\hat{\mathbf{u}}}_{eq} + \hat{\mathbf{u}}_{eq} = \mathbf{u} \tag{35}$$

where τ is the time constant of the low pass filter. The main idea, used in the design stage of the low pass filter, is that low frequencies determine the characteristics of the signal and high frequencies come from unmodeled dynamics. Using such estimation minimizes the need for system information for the control input calculation. Finally then, the control input results in,

$$\mathbf{u}(t) = \hat{\mathbf{u}}_{eq}(t) + [GB]^{-1}[\Gamma]\boldsymbol{\sigma}\,. \tag{36}$$

4. Numerical results

Numerical test results for the two-arm robotic system are presented in this section. For comparison, the numerical results obtained using the PID controller, also are presented. The PID controller was selected since it is widely used in industry. The control rule for the PID controller is

$$u(t) = K_p\left(e(t) + \tau_d \frac{d\,e(t)}{dt} + \frac{1}{\tau_i}\int_0^t e(t)\,dt \right) \tag{37}$$

where the K_p is the proportional gain, τ_d is the derivative time and τ_i is the integral time. The PID controller was tuned by trial and error at the design stage. The SMC without the chattering-free term (SMC_S) also was used, for comparative purpose as well. Its design procedure is similar to that for the designed SMC controller given in Section 3. For the SMC_S, a different Lyapunov function derivative is used such that

$$\dot{\mathbf{v}} = -\boldsymbol{\sigma}^{\mathbf{T}}[\Gamma]\,sign(\boldsymbol{\sigma}) < 0\,; \tag{38}$$

then the control law is found as

$$\mathbf{u}(t) = \hat{\mathbf{u}}_{eq}(t) + [GB]^{-1}[\Gamma]\,sign(\boldsymbol{\sigma})\,. \tag{39}$$

Here, $sign(\cdot)$ is the signum function. The parameters of the designed controllers are given in the Appendix.

In order to test the robustness of the designed controllers, normally distributed noise components were introduced to the related joints. These components were considered as external disturbance torques w_i (i = 1,2,3,4) acting on the related joints and they are represented in Fig. 5. Additionally, in order to test the performance of the designed controllers in the face of parameter variations, a sudden change in the mass of the load as seen in Fig. 5, also was introduced.

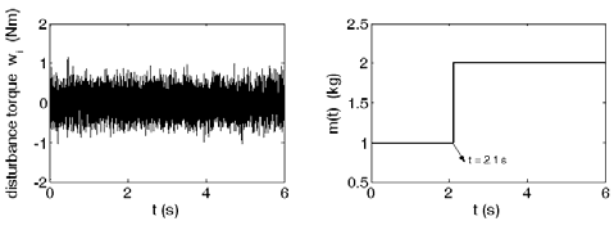

Fig. 5. Disturbance torques and mass variation of load.

There are two stages in the motion of the robot arms, namely approaching and transportation. Initially, in the present investigations, the robot arms were at rest and the corresponding initial values of the joint angles were $\theta_1(0) = 0$, $\theta_2(0) = \pi/2$, $\theta_3(0) = \pi$ and $\theta_4(0) = -\pi/2$. In the first part of the motion, the robots were approaching to the load and in the second part of the motion the robot arms handled the load and transported it to its new location. The reference trajectories for the robot arms for the approaching motion are given in Eqs. (40)-(43). Additionally, the reference trajectories for the coordinates of the load center during the transportation motion are defined in Eqs. (44)-(45):

$$x_{p1r}(t) = x_{f1} + (x_{i1} - x_{f1})\exp(-50t^3) \tag{40}$$

$$y_{p1r}(t) = y_{f1} + (y_{i1} - y_{f1})\exp(-50t^3) \tag{41}$$

$$x_{p2r}(t) = x_{f2} + (x_{i2} - x_{f2})\exp(-50t^3) \tag{42}$$

$$y_{p2r}(t) = y_{f2} + (y_{i2} - y_{f2})\exp(-50t^3) \tag{43}$$

$$x_{mr}(t) = \begin{cases} x_i\ ;\ t < 2 \\ x_f + (x_i - x_f)\exp(-50(t-2)^3)\ ;\ t \geq 2 \end{cases} \tag{44}$$

$$y_{mr}(t) = \begin{cases} y_i\ ;\ t < 2 \\ y_f + (y_i - y_f)\exp(-50(t-2)^3)\ ;\ t \geq 2 \end{cases} \tag{45}$$

Here p_1 and p_2 denote the endpoints of the first and second robot arms, respectively. Also, in the approaching motion, $(x_{i1}, y_{i1}), (x_{i2}, y_{i2})$ are the initial coordinates and $(x_{f1}, y_{f1}), (x_{f2}, y_{f2})$ are the final coordinates of the endpoints of the robot arms. Similarly, (x_i, y_i) and (x_f, y_f) are the initial and final coordinates of the load for the transportation motion. The initial and final coordinates of the load and robot arm tips are given in the Appendix. The approaching motion was accomplished by the 2nd second, at which time the transportation motion initiated. The motion of the robot arms and the transportation of the load, for the SMC case, are depicted in Fig. 6 The dotted lines represent the approaching stage and the solid lines stand for the transportation stage of motion.

The reference angles for the controllers were obtained by inverse kinematics using the desired trajectory for the load.

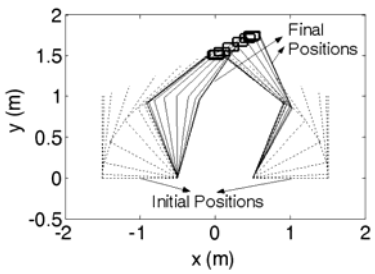

Fig. 6. Motion of the robot arms.

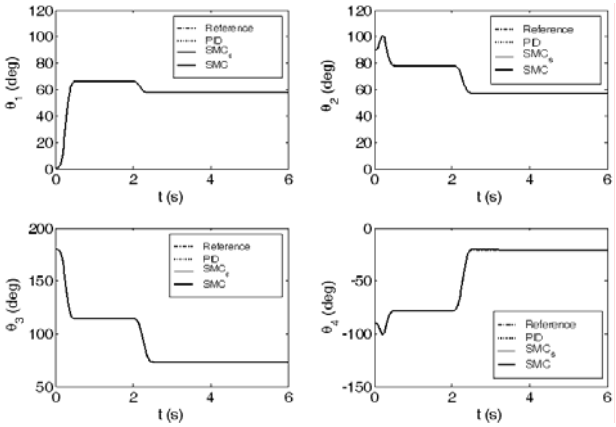

Fig. 7. The reference and the actual joint angles.

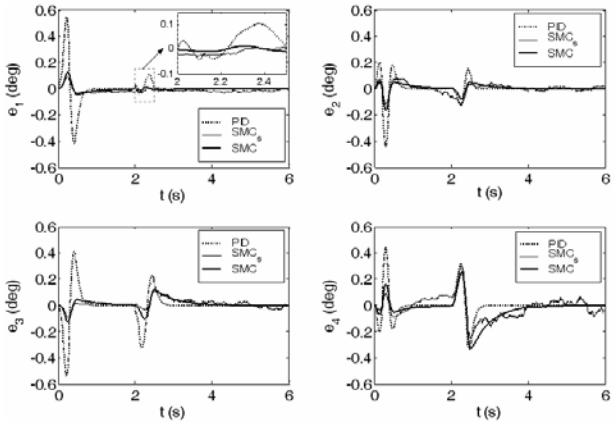

Fig. 8. Tracking errors of the related joint angles.

These reference angles, along with the PID and sliding-mode-controlled joint angles, are given in Fig. 7. It can be seen that both of the robot arms tracked their trajectory successfully, given that the reference and actual angle values overlapped.

The tracking errors for the related joint angles are shown in Fig. 8. For all of the joints, the maximum tracking error magnitudes were below 0.5 degrees, indicating the success of the PID, SMC_S and SMC. Additionally, it should be noted that even though there existed external disturbances on the joints and there was a sudden change in the mass of the load, with the designed SMC_S and SMC the robot arms tracked their specified trajectories with higher accuracy than with the PID controller. Also it should be noted that, for the PID controlled case, there were changes in the error magnitudes at $t = 2.1$ s which was due to the sudden mass variation of the load. In contrast, for the sliding mode controlled cases there was no change in the tracking error magnitudes at $t = 2.1$ s that verifies the robustness of the sliding mode controllers. Also, the figure shows that there was a chattering effect for SMC_S due to the sign term whereas in the SMC case there was no such effect.

Fig. 9 displays the tracking errors of the endpoints of the robot arms for the PID, SMC_S and SMC cases. It is evident that the SMC_S and SMC showed a better performance in accurate trajectory tracking than did the PID controller. Yet, as was the

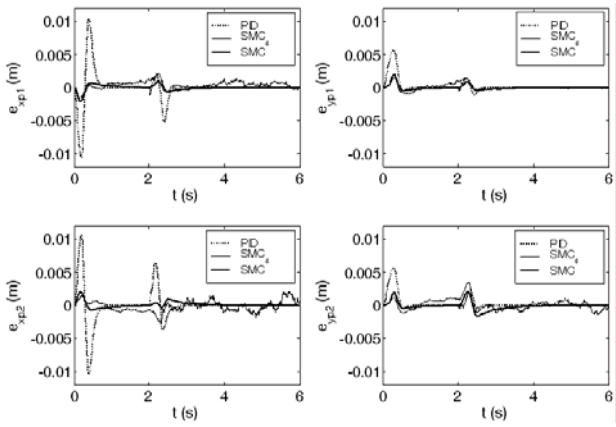

Fig. 9. Tracking errors of the endpoints of the robot arms.

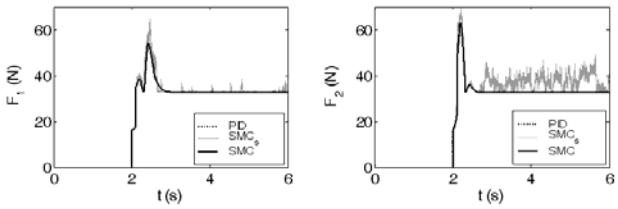

Fig. 10. Interaction forces.

case with the tracking errors of the joint angles (Fig. 8), chattering was observed for the tracking errors of the endpoints of the robot arms in the SMC_S case.

The variations of the magnitudes of the interaction forces F_1 and F_2 versus time for the PID and sliding mode controlled cases are given in Fig. 10. Both forces had zero magnitudes during the $0 \le t \le 2$ time interval since there was no interaction between the load and the robot arms during the approaching motion. Then, in the second part of the motion, the load was handled and forces accordingly started to act. The increase in the magnitudes of the forces at t = 2.1s was due to the increase of the mass of the load. At the end of the motion, it was observed that there existed residual force for both F_1 and F_2, due to the weight of the load. In fact the sum of these residual forces was equal to $m(t)g/\mu$.

The joint torques produced by the PID, SMC_S and SMC and acting on the related joints, are plotted in Fig. 11. The changes in the torque magnitudes at $t = 2$ s was due to the load handling which produced interaction forces at the contact points between the load and the tip of the robot arms. The desired non-chattering control torque action was realized during the load approaching and transportation actions thanks to the proposed SMC whereas for the SMC_S case there exists chattering which potentially can harm the mechanical components of the system.

Finally, Integral of Squarred Error (ISE) performance indices were calculated for the joint errors and torques, and they are tabulated in Table 1 and Table 2. Here, ISE (e_i) represents the tracking performance for the related link and ISE (u_i) denotes the control effort used for the actuation of the related link. Af-

Table 1. ISE values for tracking errors.

	ISE (e_1) $\times 10^{-5}$	ISE (e_2) $\times 10^{-5}$	ISE (e_3) $\times 10^{-5}$	ISE (e_4) $\times 10^{-5}$
PID	1.75	0.90	2.37	1.65
SMC	0.08	0.17	0.29	1.57
PID[1]	1.20	0.62	1.64	1.14
SMC[1]	0.07	0.13	0.24	1.00
PID[2]	2.75	1.42	3.75	2.60
SMC[2]	0.10	0.24	0.39	2.41

[1] Γ_j and K_{pj} are increased by 20%
[2] Γ_j and K_{pj} are decreased by 20%

Table 2. ISE values for control torques.

	ISE (u_1) $\times 10^4$	ISE (u_2) $\times 10^4$	ISE (u_3) $\times 10^4$	ISE (u_4) $\times 10^4$
PID	5.95	1.64	8.61	3.82
SMC	5.85	1.61	8.48	3.78
PID[1]	5.93	1.64	8.59	3.81
SMC[1]	5.86	1.61	8.52	3.76
PID[2]	5.98	1.65	8.65	3.84
SMC[2]	5.84	1.62	8.47	3.79

[1] Γ_j and K_{pj} are increased by 20%
[2] Γ_j and K_{pj} are decreased by 20%

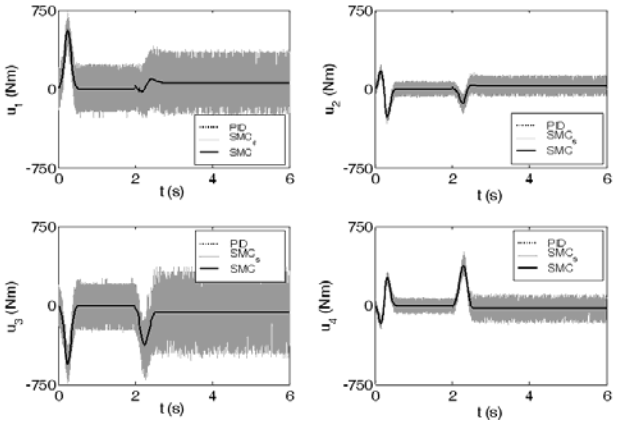

Fig. 11. Applied joint torques.

ter investigating those performance indices, it was clear that by the use of the SMC, the ISE (e_i) value was reduced for all the links without increasing the ISE (u_i). This verifies the effectiveness of the SMC. Additionally, the performances of the PID and SMC with different control gains were analyzed. To that end, the K_{pj} and Γ_j (j = 1,2,3,4) values were increased by 20% for one case and decreased by 20% for another case, as depicted in Tables 1 and 2 as PID[1], SMC[1] and PID[2], SMC[2], respectively. Upon examining those performance indices, it was apparent that the SMC outperformed the PID, all of the tracking errors having been smaller in the former case. Furthermore, it bears noting again that the SMC, in increasing tracking performance for different control gains, does not require more control effort than the PID controller.

5. Conclusions

In this study, a dual-arm robotic system for load transportation tasks was evaluated. Since reliability and robustness are the key desirable properties for that type of system, a controller designed to ensure them was investigated. In fact, according to an analysis of the numerical results, the sliding mode controller (SMC) provided accurate trajectory tracking, along with safe handling and transportation, even with parameter variations and external disturbances. Moreover, calculated trajectory tracking errors showed that the SMC performed more accurately than the widely used conventional PID controller. In light of these findings, the SMC can be recommended for applications requiring high accuracy and safe handling.

References

[1] Y. F. Zheng and J. Y. S. Luh, Optimal load distribution for two industrial robots handling a single object, *IEEE International Conference on Robotics and Automation*, Philadelphia, USA (1988) 344-349.

[2] P. Dauchez, X. Delebarre, Y. Bouffard and E. Degoulange, Task modeling and force control for a two-arm robot, *IEEE International Conference on Robotics and Automation*, Sacramento, California, (1991) 1702-1707.

[3] Q. Xue, A. A. Maciejewski and P. C.-Y. Sheu, Determining the collision-free joint space graph for two cooperating robot manipulators, *IEEE Transactions on Systems, Man, and Cybernetics,* 23 (1) (1993) 285-294.

[4] A. Kron and G. Schmidt, Haptic telepresent control technology applied to disposal of explosive ordnances: Principles and experimental results, *IEEE International Symposium on Industrial Electronics*, Dubrovnik, Croatia (2005) 1505-1510.

[5] C. R. Carignan and D. L. Akin, Cooperative control of two arms in the transport of an inertial load in zero gravity, *IEEE Transactions on Robotics and Automation,* 4 (4) (1988) 414-419.

[6] A. S. Al-Yahmadi, J. Abdo and T. C. Hsia, Modeling and control of two manipulators handling a flexible object, *Journal of the Franklin Institute,* 344 (2007) 349-361.

[7] J.-F. Liu and K. Abdel-Malek, Robust control of planar dual-arm cooperative manipulators, *Robotics and Computer Integrated Manufacturing,* 16 (2000) 109-119.

[8] M. Uchiyama, N. Iwasawa and K. Hakomori, Hybrid position/force control for coordination of a two-arm robot, *IEEE International Conference on Robotics and Automation*, Raleigh, USA (1987) 1242-1247.

[9] K. Laroussi, H. Hemami and R. E. Goddard, Coordination of two planar robots in lifting, *IEEE Journal of Robotics and Automation,* 4 (1) (1988) 77-85.

[10] S.-T. Lin and A.-K. Huang, Position-based fuzzy force control for dual industrial robots, *Journal of Intelligent and Robotic Systems,* 19 (4) (1997) 393-409.

[11] V. I. Utkin, Variable structure systems with sliding modes. *IEEE Transactions on Automatic Control* 22 (1977) 212-222.
[12] N. Yagiz and Y. Hacioglu, Fuzzy sliding modes with moving surface for robust control of a planar robot, *Journal of Vibration and Control,* 11 (3) (2005) 903-922.
[13] P. Herman, Sliding mode control of manipulators using first-order equations of motion with diagonal mass matrix, *Journal of the Franklin Institute,* 342 (2005) 353-363.
[14] M. L. Corradini and G. Orlando, Control of mobile robots with uncertainties in dynamical model: a discrete time sliding mode approach with experimental results, *Control Engineering Practice,* 10 (2002) 23-34.
[15] S. Yannier, A. Sabanovic, A. Onat and M. Bastan, Sliding mode based obstacle avoidance and target tracking for mobile robots, *Proceedings of the IEEE International Symposium on Industrial Electronics*, June 20-23, Dubrovnik, Croatia (2005) 1489-1494.
[16] G. Herrmann, S. K. Spurgeon and C. Edwards, A model-based sliding mode control methodology applied to the HDA-plant, *Journal of Process Control,* 13 (2003) 129-138.
[17] E. M. Jafarov and R. Tasaltin, Robust sliding mode control for the uncertain MIMO aircraft model F-18, *IEEE Transactions on Aerospace and Electronic Systems,* 36 (4) (2000) 1127-1141.
[18] J. H. Park and Y. J. Lee, Robust visual servoing for motion control of the ball on a plate, *Mechatronics,* 13 (7) (2003) 723-738.
[19] C. Edwards and S. K. Spurgeon, *Sliding Mode Control: Theory and Applications*, Taylor & Francis (1998).
[20] Q. P. Ha, D. C. Rye and H. F. Durrant-Whyte, Fuzzy moving sliding mode control with application to robotic manipulators, *Automatica,* 35 (1999) 607-616.
[21] V. Utkin, J. Guldner and J. Shi, *Sliding Mode Control in Electromechanical Systems,* Taylor & Francis (1999).

Appendix

i) Numerical parameters of two-arm robotic system:

$m_i = 1$ [kg]	$\mu = 0.3$
$I_i = 0.0833$ [kgm^2]	$b_i = 100$ [Nms]
$L_i = 1$ [m]	$d_1 = 0.2$ [m]
$k_i = 0.5$ [m]	$d_2 = 1$ [m]
$m\ (t)$ = See Fig. 5	

$i = 1,2,3,4$

ii) Constant coefficients A_i used in the equations of motion of robot arms:

$$A_1 = m_1 k_1^2 + m_2 L_1^2 + I_1 \quad (A.1)$$

$$A_2 = m_2 k_2^2 + I_2 \quad (A.2)$$

$$A_3 = m_2 L_1 k_2 \quad (A.3)$$

$$A_4 = m_3 k_3^2 + m_4 L_3^2 + I_3 \quad (A.4)$$

$$A_5 = m_4 k_4^2 + I_4 \quad (A.5)$$

$$A_6 = m_4 L_3 k_4 \quad (A.6)$$

iii) Numerical parameters of controllers:

SMC	SMC_S	PID
$\tau_j = 0.001$	$\tau_j = 0.001$	$K_{pj} = 30000$
$\Gamma_j = 1000$	$\Gamma_j = 70$	$\tau_{ij} = 0.1$
$\lambda_j = 2$	$\lambda_j = 2$	$\tau_{dj} = 0.01$

$j = 1,2,3,4$

iv) Initial and final coordinates of load and robot arm tips:

Robot Arm Tips	Load
$(x_{i1},y_{i1}) = (1.5,1)$ [m]	$(x_{is},y_{is}) = (0,1.5)$ [m]
$(x_{f1},y_{f1}) = (0.1,1.5)$ [m]	$(x_{fs},y_{fs}) = (0.5,1.75)$ [m]
$(x_{i2},y_{i2}) = (-1.5,1)$ [m]	
$(x_{f2},y_{f2}) = (-0.1,1.5)$ [m]	

Nurkan Yagiz received his B.S. and M.S. degrees from the Department of Mechanical Engineering, Middle East Technical University, Ankara, Turkey, in 1984 and 1986, respectively, and his Ph.D. degree from the Department of Mechanical Engineering, Faculty of Engineering, Istanbul University, Istanbul, Turkey, in 1993. He is currently a Professor with the Department of Mechanical Engineering, Faculty of Engineering, Istanbul University. His research areas include modeling and control of vehicle systems, control of structural vibrations, and nonlinear control theory.

Yuksel Hacioglu received his B.S., M.S. and Ph.D. degrees from the Department of Mechanical Engineering, Faculty of Engineering, Istanbul University, Istanbul, Turkey, in 2002, 2004 and 2009, respectively. He is currently an Assistant Professor with the Department of Mechanical Engineering, Faculty of Engineering, Istanbul University. His research areas include modeling and control of robotic manipulators and vehicle suspension systems, nonlinear control theory, and fuzzy logic.

Yunus Ziya Arslan received his B.Sc. degree in 2002, his M.Sc. degree in 2005 and his Ph.D. degree in 2009, all from the Department of Mechanical Engineering, Faculty of Engineering, Istanbul University, Istanbul, Turkey. He is currently an Assistant Professor with the Department of Mechanical Engineering, Faculty of Engineering, Istanbul University. His research areas include biomechanics of musculoskeletal systems, as well as modeling and control of robotic manipulators.